EVALUATION OF DIFFERENT TURBULENCE MODELS TO PREDICT A TURBULENT FREE JET

C. C. Pérez; C. V. Barreto; G. Lopes; J. N. E. Carneiro, J. K. Abrantes, J. M. Barros Jr, A. O. Nieckele
Dept. Engenharia Mecânica – Pontifícia Universidade Católica do Rio de Janeiro, PUC/Rio
Rua Marquês de São Vicente, 225 – Gávea, 22453-900, Rio de Janreiro, RJ, Brazil
ccperez@ mec.puc-rio.br; cvb-prg@ mec.puc-rio.br; glopes@ mec.puc-rio.br
carneiro@ mec.puc-rio.br; abrantes@ mec.puc-rio.br; jmb@ mec.puc-rio.br; nieckele@mec.puc-rio.br

Abstract. *Turbulent free jet flows are present on several processes and technological applications, also being widely used as a benchmark problem for turbulent models validation. In the present work, a numerical study was carried out using the finite-volume method to evaluate the performance of different types of turbulence models, including κ–ε Standard, κ–ε Realizable, κ–ε RNG, κ–ω SST and Reynolds Stress models to predict this type of flow. The mean velocity and Reynolds stresses profiles obtained with the different models were compared to each other and with available experimental and DNS data. All models presented qualitatively similar results. The condition of self-similarity was attained, but large discrepancies were observed in relation to experimetal and DNS data.*

Keywords*: Turbulent Axisymmetric Free Jet, Turbulence Models, Self-Similarity*

1. Introduction

The axisymmetric jet flow has been widely used in the study of turbulence. It has become a benchmark problem for turbulence models validation as well as measurements techniques, being a good prototype for free-shear flows. This is evidenced by the great number of publications concerning experimental, theoretical and numerical analysis for this configuration. Also, several practical applications can be found, such as swirling flows, impinging jets, burners, and propulsion systems, among others.

Experimental investigations of a jet flow started being conducted in the early 40`s. The failure of turbulence intensities to attain self-preservation in these early works motivated the measurement of velocity and turbulent stresses by Wygnanski and Fielder (1969), using linearized hot wires.

Panchapakesan and Lumley (1993) performed experimental measurements in a turbulent round jet of air discharging into quiescent air using x-wire and hot-wire probes. The consistency of the measurements with the equations of motion was verified assessing the momentum flux (found to be of approximately 5% of the nozzle input) and the integral of the radial diffusive flux of turbulent kinetic energy across the jet (found to be close to zero).

One of the standard references concerning the turbulent free jet investigation is the experimental work of Hussein *et al* (1994), in which the quantities were measured using both LDA and hot wire anemometer. The work presents a theoretical analysis of the problem by properly fitting the experimental data into the equations of motion and verifying the integral conservation of momentum, considering both the mean and second order moments of velocity – the latter having a smaller contribution for the overall balance. This constitutes an important test to verify whether the experiment reasonably reproduces an axisymmetric jet into an infinite environment.

The developing region was experimentally investigated by Weisgraber and Liepmann (1998) through use of DPIV (Digital Particle Image Velocimetry). Comparisons with LDA data from Hussein *et al.* (1994) were made, contrasting transitional and self-similar regions.

Large Eddy Simulations (LES) of spatially developing circular jet were carried out by Olsson and Fuchs (1995). Different cases were simulated to study the effect of Reynolds number, spatial resolution and SGS (sub-grid scales) models.

Boersma *et al.* (1998) investigated the effect of lateral boundary conditions on the solution, obtaining different flow patterns for the laminar free jet, implying that a larger domain may be needed in order to "isolate" the region of interest from boundary influence. To investigate the effect of the inlet velocity profile on the self-similar solution, Direct Numerical Simulation (DNS) was carried out for the turbulent jet. Good agreement was obtained with experimental work of Panchapakesan and Lumley (1993) and Hussein *et al.* (1994), but details of the self-similarity were found to be affected both by inlet conditions and by the scaling used to non-dimensionalize the results.

Mcllwain and Pollard (2001) analyzed the near field of a round jet with and without swirl, by means of Large Eddy Simulations (LES). Good agreement was obtained with previous simulations (Olsson and Fuchs, 1995) and experimental data. Merci and Dick (2002) investigated the performance of a modified k-ε model in the prediction of different types of flows. In particular for plane and round jets, it appears that the modified ε-equation improved the agreement of the results with experimental data of Panchapakesan and Lumley (1993). The standard k-ε model overpredicts radial profiles of mean velocity and turbulent shear stresses.

Recently, Abrantes (2005) obtained a detailed set of data for the free jet employing the LDV technique. The data were compared with Hussain *et al* (1994) measurements and showed excellent agreement.

The objective of the present work is to access the performance of different turbulence models in predicting the

characteristics of an axisymmetric free jet, employing the commercial software Fluent, v.6.2. The average velocities as well as the Reynolds stresses are determined and it is investigated whether the different models are capable of predicting self similar solutions far from the jet.

2. Mathematical Modeling

To determine the turbulent flow field, the Reynolds-averaged mass and *momentum* equations were solved. This approach is based on decomposing the velocity as $u_i = \overline{u_i} + u_i'$, where $\overline{u_i}$ is the average velocity and u_i' the velocity fluctuation. The average *momentum* equation (RANS), for a steady state incompressible flow is given by

$$\frac{\partial}{\partial x_j}\left(\rho\,\overline{u_i}\;\overline{u_j}\right) = -\frac{\partial p}{\partial x_i} + \frac{\partial}{\partial x_j}\left[\mu\left(\frac{\partial \overline{u_i}}{\partial x_j} + \frac{\partial \overline{u_j}}{\partial x_i}\right)\right] + \frac{\partial\left(\rho\,\overline{u_i'\,u_j'}\right)}{\partial x_j} \tag{1}$$

where ρ is the density, μ is the molecular viscosity, p is the pressure and x_i are the directions in the coordinate system. Equation (1) has the same form of the Navier-Stokes equation, but now it has an additional term, the turbulent Reynolds stress term, $-\rho\overline{u_i'\,u_j'}$, representing the influence of the fluctuation on the average flow, which must be modeled in order to close Eq. (1).

The commercial software Fluent offers a wide selecting of turbulence models, ranging from one differential equation model (Spalart Allmaras), two differential equations models (standard, RNG and Realizable κ–ε; and standard and shear stress transport κ–ω models and v^2-f model) and Reynolds stress model (RSM) to Detached Eddy Simulation (DES) and LES (Large Eddy Simulation). Although several RANS models were employed to predict the flow field, at the present work, the five models that presented the best results were selected. Four models are based on the Boussinesq approach (Hinze, 1975), which employs the concept of turbulent eddy viscosity μ_t, and the fifth model involves the direct determination of the Reynolds Stresses (RSM model). The main advantage of the turbulent viscosity models, when compared to the RSM model, is the lower computational cost, because only one or two additional equations are solved.

2.1 Turbulent Viscosity Models

The Boussinesq approach employs the concept of turbulent eddy viscosity μ_t to relate the Reynolds Stress with the rate of deformation of the mean flow, as

$$\rho\overline{u_i'\,u_j'} = \mu_t\left(\frac{\partial \overline{u_i}}{\partial x_j} + \frac{\partial \overline{u_j}}{\partial x_i}\right) - \frac{2}{3}(\rho\,\kappa)\delta_{ij} \tag{2}$$

where κ is the turbulent kinetic energy and δ_{ij} is the Kronecker delta. The last term is added to account for dynamic pressure fluctuations.

The models selected to be presented here were: κ–ε Standard (Launder and Spalding, 1974), κ–ε RNG (Speziale *et al.*1992), κ–ε Realizable (Shih *et al*. 1995) and κ–ω SST models (Menter,1994). The turbulent viscosity for the high Reynolds number form of the κ–ε models and κ–ω model are defined as

$$\mu_t = \rho C_\mu \frac{\kappa^2}{\varepsilon} \qquad ; \qquad \mu_t = \rho\frac{\kappa}{\omega} \tag{3}$$

where κ is the turbulent kinetic energy, ε is its dissipation rate and ω is the specific dissipation rate. C_μ is an empirical constant equal to 0.09 for the κ–ε standard and 0.085 for the κ–ε RNG. For the κ–ε Realizable, C_μ is a function of the mean flow deformation rate S_{ij} and mean rate of rotation tensor Ω_{ij}, as

$$C_\mu = \left[4.04 + \sqrt{6}\,\cos\left(\frac{\cos^{-1}(\sqrt{6}\,W)}{3}\right)\frac{\kappa\,U^*}{\varepsilon}\right]^{-1} \quad ; \quad U^* = \sqrt{S_{ij}S_{ij} + \Omega_{ij}\Omega_{ij}} \quad ; \quad W = \frac{S_{ij}S_{ik}S_{kj}}{S} \tag{4}$$

$$S_{ij} = \frac{1}{2}\left(\frac{\partial \overline{u_i}}{\partial x_j} + \frac{\partial \overline{u_j}}{\partial x_i}\right) \qquad ; \qquad \Omega_{ij} = \frac{1}{2}\left(\frac{\partial \overline{u_i}}{\partial x_j} - \frac{\partial \overline{u_j}}{\partial x_i}\right) \qquad ; \qquad S = \sqrt{S_{ij}S_{ij}} \tag{5}$$

Each model requires the solution of two additional transport equations: one for κ and other for ε, for the κ–ε models

and one for κ and another for ω, for the κ–ω model. All transport equations can be written in the general form shown in Eq. (6), where ϕ is the transport variable:

$$\frac{\partial}{\partial x_j}\left(\rho\,\phi\,\overline{u_j}\right)=\frac{\partial}{\partial x_j}\left(\Gamma_\phi\,\frac{\partial\phi}{\partial x_j}\right)+G_\phi-Y_\phi \tag{6}$$

where Γ_ϕ represents the diffusivity of ϕ, G_ϕ represents the production term and Y_ϕ represents the destruction. In general, the diffusivity term is defined as

$$\Gamma_\phi=\mu+\mu_t/\sigma_\phi \tag{7}$$

where σ_ϕ is the turbulent Prandtl number, and assume the following values: (i) κ–ε Standard: σ_κ=1 , σ_ε=1.3 (ii) κ–ε Realizable: σ_κ=1, σ_ε=1.2 (iii) κ–ω SST: σ_κ=2, σ_ε=2. For the κ–ε *RNG* model, the diffusion is based on the inverse effective Prandtl numbers α_ϕ:

$$\Gamma_\phi=\alpha_\phi(\mu+\mu_t) \quad \text{where} \quad \alpha_\kappa=\alpha_\varepsilon=1.393 \text{ (for high Reynolds number).} \tag{8}$$

The main difference between the turbulent viscosity models are the turbulent viscosity definition, given by Eq. (3), and how the production and destruction terms of the turbulent quantities in their respective transport equation are obtained. Table 1 shows the production and destruction terms for each model. The term η is the ratio of turbulence to mean strain, $\eta=S\,\kappa/\varepsilon$. D_ω is the cross diffusion term, due to the transformation of the κ–ε equation in a κ–ω equation.

Table 1. Differences between the mathematical models

Model	**Production**		**Destruction**	
	κ equation	ε equation	κ equation	ε equation
κ–ε *Standard*	$G_\kappa=2\,\mu_t\,S^2$	$G_\varepsilon=C_1\frac{\varepsilon}{\kappa}G_\kappa$; C_1=1.44	$Y_\kappa=\rho\varepsilon$	$Y_\varepsilon=\rho C_2\frac{\varepsilon^2}{\kappa}$, C_2=1.92
κ–ε *RNG*	$G_\kappa=2\,\mu_t\,S^2$	$G_\varepsilon=C_1\frac{\varepsilon}{\kappa}G_\kappa$; C_1=1.44	$Y_\kappa=\rho\varepsilon$	$Y_\varepsilon=(\rho C_2+R_\varepsilon)\frac{\varepsilon^2}{\kappa}$; C_2=1.68 ; $R_\varepsilon=C_\mu\,\rho\,\eta^3(1-\eta/4.38)/(1+0.012\,\eta^3)$
κ–ε *Realizable*	$G_\kappa=2\,\mu_t\,S^2$	$G_\varepsilon=\rho C_1 S\varepsilon$; $C_1=max[0.43,\eta/(\eta+5)]$	$Y_\kappa=\rho\varepsilon$	$Y_\varepsilon=\rho C_2\frac{\varepsilon^2}{\kappa+\sqrt{\mu\varepsilon/\rho}}$ C_2=1.9
	κ equation	ω equation	κ equation	ω equation
κ–ω *SST*	$G_\kappa=2\,\mu_t\,S^2$	$G_\omega=\frac{\omega}{\kappa}G_k$	$Y_\kappa=\beta^*\rho\kappa\omega$; β^*=0.09	$Y_\omega=\beta\,\rho\,\omega^2-D_\omega$; $D_\omega=\frac{2\sigma_\omega\rho}{\omega}\frac{\partial\kappa}{\partial x_j}\frac{\partial\omega}{\partial x_j}$; β=0.0828 ; σ_ω=1.168

The *k*-ω SST model blends the formulation of *k*-ω model in near-wall regions with the free stream independence of the κ-ε model in the far field. Thus, for the present analysis, the *k*-ω SST model is similar to the κ–ε model, since there are no walls present. However, the turbulent viscosity and the constants are different; furthermore, a cross diffusion term was added to the ω equation. The variables β and β^* that appear in the destruction terms of ω depend on the distance to the closest wall, which was assumed to be infinite in the calculations with no walls in the domain, resulting in constant values. This has happened because most of the additional terms that are responsible for taking into account the proximity of a wall were neglected. The model behaved neither exactly like the standard *k*-ω model nor the κ-ε model, because part of a cross-diffusion term still remained non-zero. For the present problem, the κ–ω SST model provided a greater stability in the convergence process than the standard *k*-ω model, which is not presented.

2.2 Reynolds Stress Model

The Reynolds Stress Model calculates all the components of the tensor $\overline{u_i'\,u_j'}$ using transport equations. The

computing effort of this model is much higher than the eddy viscosity models; however, it is capable of predicting turbulent anisotropy, unlike the former models. The RSM transport equation has the same form as the general Eq. (6), where the dependent variable is $\phi = \overline{u_i' u_j'}$:

$$\frac{\partial \rho \overline{u_k} \ \overline{u_i' u_j'}}{\partial x_k} = \frac{\partial}{\partial x_k}\left[\left(\mu + \frac{\mu_t}{\sigma_\kappa}\right)\frac{\partial \overline{u_i' u_j'}}{\partial x_k}\right] + P_{ij} + \Pi_{ij} - \frac{2}{3}\rho\,\varepsilon\,\delta_{ij} \tag{9}$$

In equation (9), the stress production term P_{ij} and pressure strain term Π_{ij} (Gibson & Launder, 1978; Fu *et al*. 1987; and Launder, 1989). are given by:

$$P_{ij} = -\rho\left(\overline{u_i' u_k'}\frac{\partial \overline{u_j}}{\partial x_k} + \overline{u_j' u_k'}\frac{\partial \overline{u_i}}{\partial x_k}\right) \quad ; \quad \Pi_{ij} = -1.8\,\rho\frac{\varepsilon}{\kappa}\left[\overline{u_i' u_k'} - \frac{2}{3}\kappa\delta_{ij}\right] - 0.6\left[(P_{ij} - C_{ij}) - \frac{2}{3}(P - C)\delta_{ij}\right] \tag{10}$$

where $P = (1/2)\ P_{kk}$ and $C = (1/2)\ C_{kk}$, where C_{ij} is the convective term, the only term on the left hand side of Eq. (9). The kinetic energy κ, when needed is obtained from

$$\kappa = \frac{1}{2}\overline{u_i' u_i'} \tag{11}$$

and ε, the dissipation rate of κ, is determined by the same ε equation of the standard κ–ε model, where the production term $G\kappa$ is determined from the Reynolds stress, thus $G_\kappa = P$. The turbulent viscosity is also the same as the κ–ε model.

3. Numerical Method

The flow field was numerically obtained with the commercial software *FLUENT*, v6.2 (2005), which is based on the Finite Volume method (Patankar, 1980). To approximate the convection/diffusion flux, the *"power-law"* scheme was employed and the pressure-velocity coupling was handled with the *SIMPLE* algorithm. The conservation equations were solved in a segregate and sequential manner. The solution was considered converged when the sum of the normalized residuals of all equations was smaller than 10^{-6}.

The computational domain was defined based on the experimental apparatus of Abrantes (2005), with a length equal to 40 *d* and 20 *d* in the *z* and *r* directions, respectively, where *d* is the diameter of the inlet jet. A non uniform mesh, refined in the region closer to the centerline of the jet, with 75000 (150 × 500) control volumes was generated with the *FLUENT* auxiliary tool *GAMBIT* (*Fluent*, 2005). A grid independent solution was assured by comparing results obtained with a finer grid (120000 control volumes, 200 × 600). Negligible differences were observed.

The size of the computational domain was also investigated with the κ–ε *Standard.* The length of the domain was double, while maintaining the radial size. Again, negligible differences were detected.

4. Problem Setup

Figure 1 shows the domain and the location of the boundaries, as well as the characteristic regions of a developing free jet. After the potential core – in which the jet centerline is not yet affected by the mixing layer - the axial velocity in the jet centerline begins to decay and the jet develops to a self-similar state, in which profiles of mean velocity and turbulent stresses plotted against the similarity variable $r/(x\text{-}x_0)$ no longer vary with the axial position. The virtual origin, x_0, is related to the end of the potential core region, and was calculated separately for each model by plotting the mean axial velocity profile along the centerline.

A velocity profile measured experimentally with LDV (Abrantes, 2005) was imposed at the inlet boundary. It corresponds to a Reynols number based on the jet exit diameter, *d*, of 21000. For the turbulence quantities, profiles of κ, ω and ε were obtained from the experimental data by using the following definitions:

$$k = \frac{1}{2}(\overline{u'^2} + \overline{v'^2} + \overline{w'^2}) \quad , \quad \varepsilon = C_\mu^{3/4}\frac{k^{3/2}}{l} , \quad \omega = \frac{k^{1/2}}{C_\mu^{1/4} l} \tag{12}$$

with the turbulence length scale *l* defined as $l = 0.07\ d$.

For the other boundaries, a pressure condition equal to 1 atm was considered. With this type of boundary condition, the fluid can leave the domain, with negligible diffusion, or enter the domain with a very low prescribed turbulence intensity.

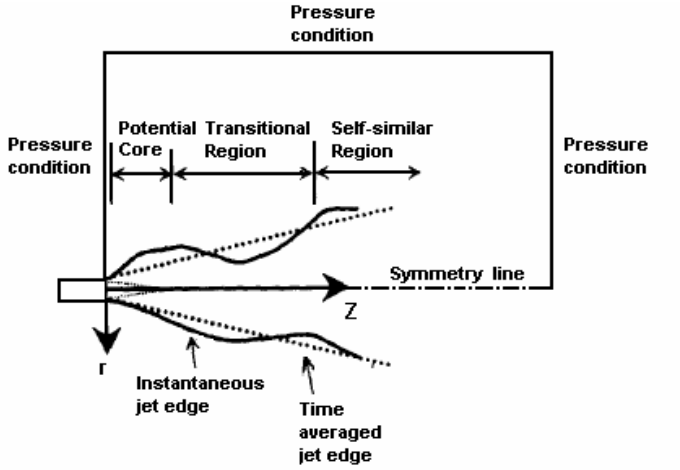

Figure 1. Schematic view of the domain, boundary conditions and flow characteristics

5.Results

In steady state numerical investigations found in literature, the κ–ε model has been mostly used. Some researchers (e.g., Merci and Dick, 2002) also investigated the performance of modified versions of the κ–ε model in order to improve the agreement with previous experimental data. In the present work, besides the standard version, two variations of the κ–ε model were also tested (κ–ε *RNG* and κ–ε *Realizable*). In addition, κ–ω *SST* and the Reynolds Stress Model (*RSM*) were also employed.

To evaluate the turbulent models selected to be tested, the turbulent stresses and the mean axial velocity obtained with the various models are compared at different position in Figs. 2, 3 and 4. It is investigated if the models are able to attain a self similar solution and their prediction are compared with available experimental and DNS data.

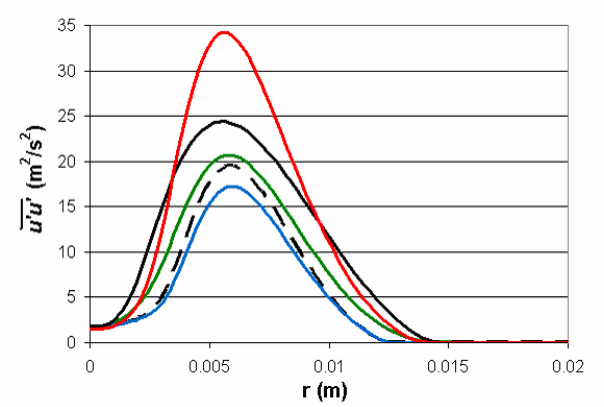

(a) normal Reynolds stress $\overline{u'u'}$

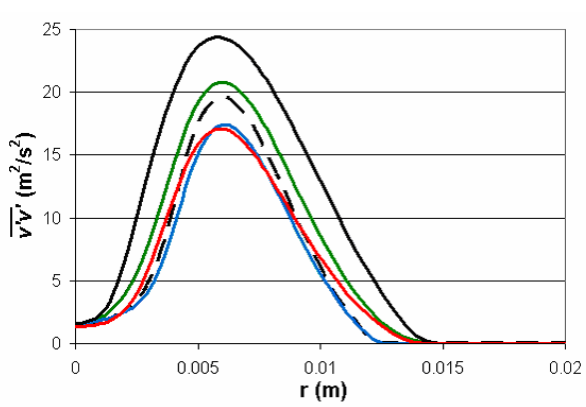

(b) normal Reynolds stress $\overline{v'v'}$

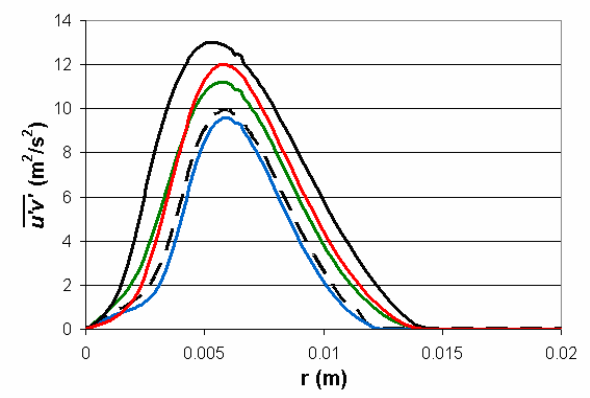

(c) shear Reynolds stress $\overline{u'v'}$

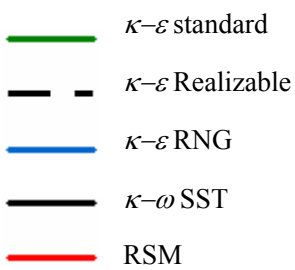

Figure 2 – Profiles of turbulent stresses for $x/d = 2$

Figure 2 presents a comparison of the turbulent stresses $\overline{u'u'}$, $\overline{v'v'}$ and $\overline{u'v'}$ profiles along the radial direction at x/d = 2. It can be observed that, although located in an axial position close to the inlet, the profiles predicted by the different models show a considerable discrepancy (one could expect that the profiles would still be strongly influenced by the imposed inlet conditions). All models agree in the prediction of the position of stresses peak values, but those values can differ as much as 100%. The positions of higher stresses are related to the generation of turbulence in the pipe wall and in the shear layer that is created. This turbulence is expected to be diffused to the centerline as the jet develops, as it will be seen later in this paper, when results for larger axial distances are to be presented.

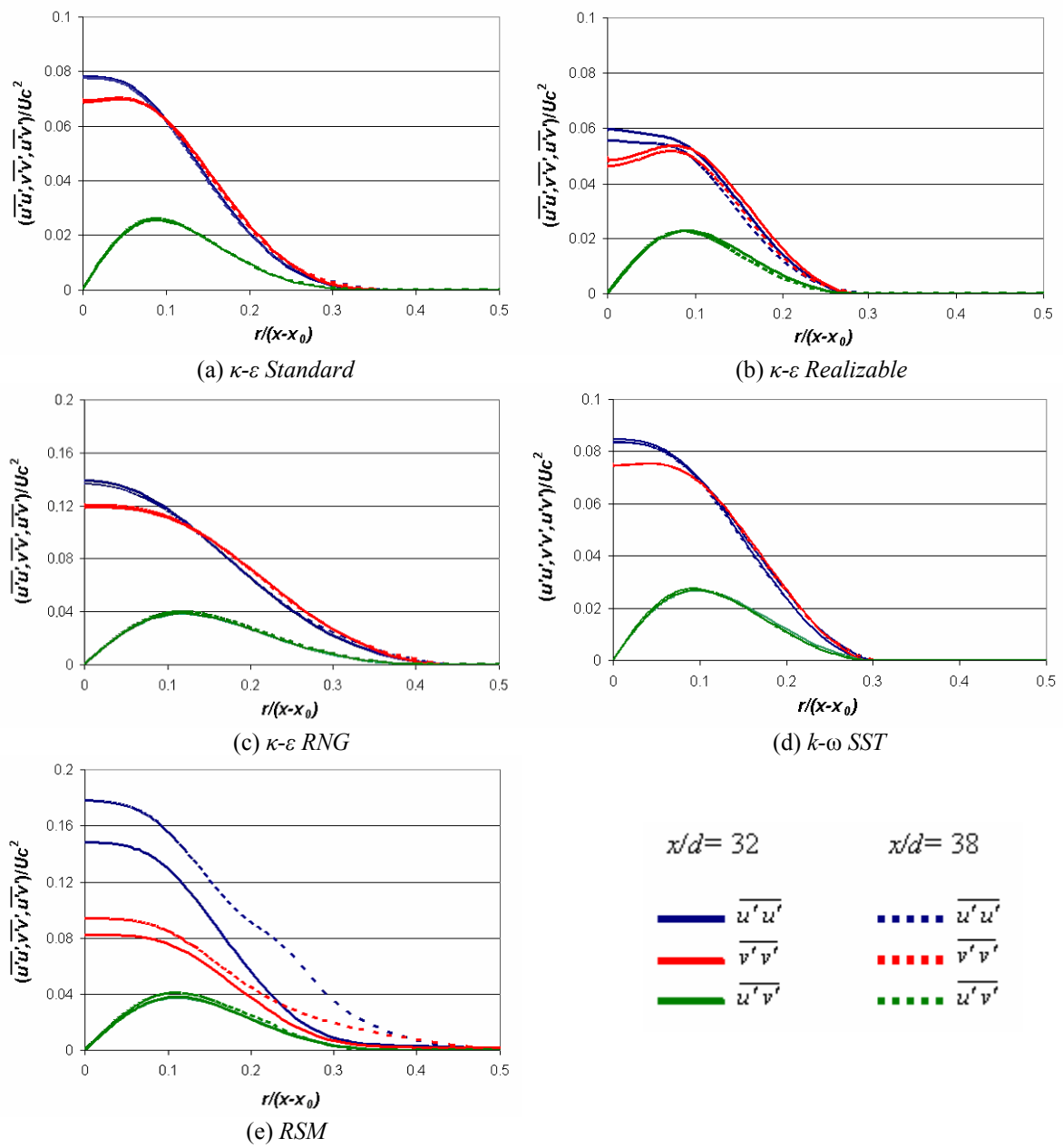

Figure 3. Self-Similar profiles of turbulent stresses for the different models

The self-similarity condition for the mean velocity is expected to be attained at high distances from the jet exit, at approximately 25 jet diameters downstream. The turbulent stresses also become self-similar, but at slightly higher distances from the jet exit. For this reason, plotting profiles of the stresses is a stricter test in order to verify the overall self-similarity. Figure 3 presents, for each model separately, profiles of turbulent stresses at two different axial positions; x/d = 32 and x/d = 38. Each color in the graphs corresponds to a different Reynolds stress. The stresses are non-dimensionalized by the axial centerline velocity U_C. The Reynolds stress profiles obtained with all models correspond to the expected. The normal stresses $\overline{u'u'}$ and $\overline{v'v'}$ are maximum at the axis and decrease as the similarity coordinate $r/(x\text{-}x_0)$ increases, while the shear stress $\overline{u'v'}$ increases, reaches a maximum at $r/(x\text{-}x_0)\approx 0.1$ and then decreases. One can observe that the self-

similarity is achieved by all turbulent viscosity models, but for the *RSM* model, the exit boundary conditions seem to have affected the results at x/d = 38. This brings out the necessity of further investigations using a larger domain for the *RSM* model, since the domain size did not affect the results of the k-ε models.

A comparison of the results obtained by the different models at x/d = 32 is presented in Fig. 4. It shows profiles of mean axial velocity ($\overline{u}$) and turbulent stresses ($\overline{u'u'}$, $\overline{v'v'}$ and $\overline{u'v'}$) – non-dimensionalized by the jet centerline velocity at the referred axial position (U_C) – plotted against the similarity variable, $r/(x\text{-}x_0)$. The results are also compared with experimental data of Hussein *et al*. (1994) and Abrantes (2005) as well as numerical DNS data from Boersma *et al*. (1998).

The mean axial velocity profiles are shown in Fig. (4a). It can be seen that the standard κ–ε, Realizable κ–ε and κ–ω SST models predicted a similar profile. The κ–ε *RNG* and *RSM* produced a reduced decay of the velocity. All models predicted a higher spreading of the jet when compared to the experimental data, pointing out that, in the numerical simulations, the diffusion of axial *momentum* in the radial direction is higher.

The Reynolds stresses are shown in Fig. 4b through Fig. 4d. It can be observed that qualitatively all models predicted a reasonable result; however, the maximum values can differ significantly from one model to another and also from the models to the experimental and DNS data. Once again, the κ–ε *RNG and RSM*, overestimated all quantities, more than the others models. A discrepancy among the experimental data and the DNS results can also be observed, probably due to difference on the turbulence intensity of the inlet jet, since this is a data difficult to measure and not very well informed.

One can note, by comparing the normal turbulent stresses profiles at x/d = 2 (Fig.2) and at x/d = 32 (Fig.4), that the turbulence intensity is diffused towards the jet axis, and therefore the position of peak values of the stresses shifts to the centerline as the axial distance from the jet axis grows.

The κ–ε *RNG* and *RSM* models seem to have overestimated the values of turbulent normal and shear stresses as well as the spreading of the jet, much more than the other models. For the other models, the discrepancies in the stress values in respect to experimental and DNS data were less significant. In fact, it is important to note that the differences between experimental and DNS data are not negligible. Considering the order of these differences, it is fair to say that the κ–ε standard, the κ–ε realizable and the κ–ω SST models presented reasonable results, obtaining the best performances among the models used in terms of computational effort and quality of results.

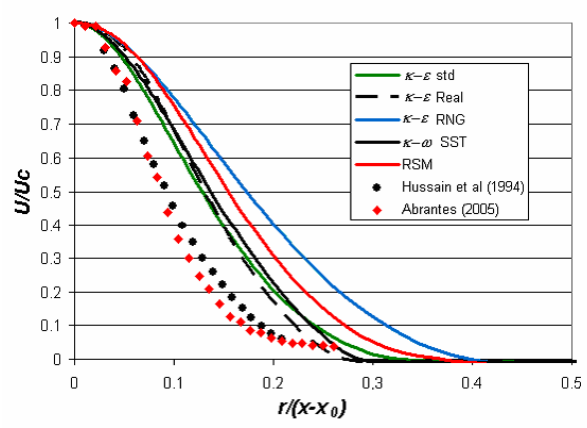

(a) mean axial velocity

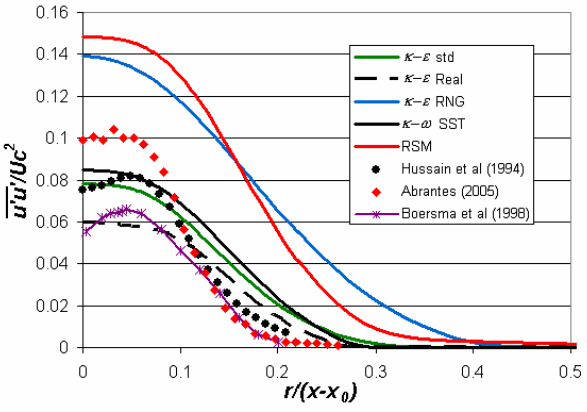

(b) normal Reynolds stress $\overline{u'u'}$

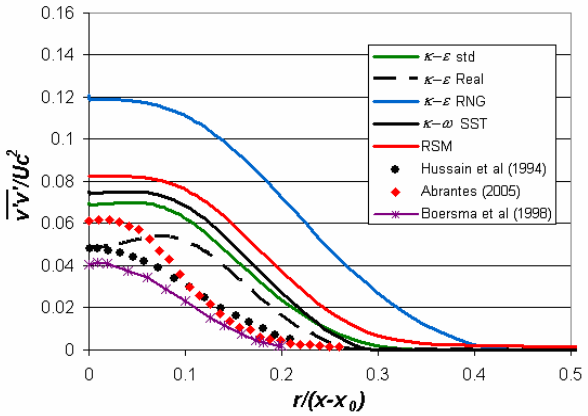

(c) normal Reynolds stress $\overline{v'v'}$

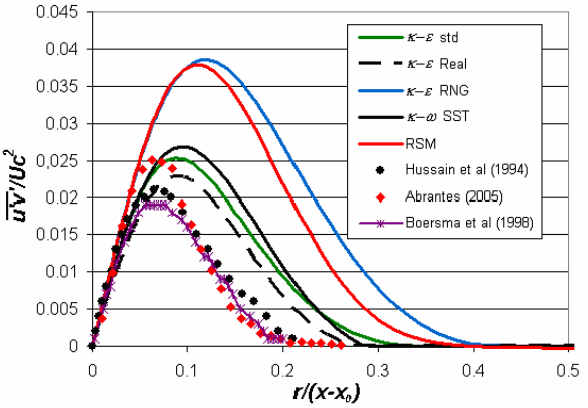

(d) shear Reynolds stress $\overline{u'v'}$

Figure 4. Mean Velocity and turbulent stresses profiles for x/d=32

6.Conclusions

In the present work, different types of turbulence models were tested to evaluate their ability to predict a free round jet. Most models predicted the expected self-similar behavior of mean velocity and turbulent stresses at large distances from the jet exit, but they seem to have reached different self-similar states, showing significant differences in the values of turbulent quantities when compared to each other.

Although no model presented a very good result, the κ–ε standard, the κ–ε realizable and the κ–ω SST models presented the best performances among the models tested. Surprisingly the *RSM* model did not predict very well the free jet flow. For this model, a reverse flow was obtained at the downstream border, indicating that the computational domain was not large enough, at least for this model. Further numerical investigation in a larger domain is recommended, especially in order to check the self-similar profiles at even higher axial distances from the jet exit.

7. Acknowledgement

The authors thank CNPq for the support during the development of this work.

8. References

Abrantes, J.K., 2005, “Estudo do Escoamento e Transferência de Calor em um Jato Espiralado Incidente”, Master’s Thesis, in portuguese, Pontifícia Universidade Católica do Rio de Janeiro – PUC-RJ.

Boersma B. J., Brethouwer G., Nieuwstadt F.T.M., 1998, “A Numerical Investigation on the effect of the inflow condition on the self-similar region of a round jet”. Physics of fluids, vol. 10, pp 899-909

Fluent Users Guide, 2005, Fluent Inc.

Fu S., Launder B.E., Leschziner M.A., 1987, “Modeling Strongly Swirling Recirculating Jet Flow with Reynolds-Stress Transport Closures”, In Sixth Symposium on Turbulent Shear Flows, Toulouse, France, 1987.

Gibson M.M., Launder B.E., 1978, “Ground Effects on Pressure Fluctuations in the Atmospheric Boundary Layer”, J. Fluid Mech., 86:491-511.

Hinze, J.O., 1975, “Turbulence”, McGraw Hill, New York.

Hussain H. J., Capp S. P. and George W. K., 1994, “Velocity Measurements in a high Reynolds number, momentum-conserving, axisymmetric, turbulent jet”, J. Fluid Mechanics, vol. 258, pp 31-75.

Launder B.E. and Spalding, D.B., 1974. "The Numerical Computation of Turbulent Flows", Computer Methods in App. Mech. and Engineering, 3, pp. 269-289.

Launder, B.E., 1989, “Second-Moment closure and its use in modeling turbulent industrial flows”, Int. Journal of Numerical Methods in Fluids, 9:963-985.

Mcllwain S., Polland A., 2002, “Large eddy simulation of the effects of mild swirl on the near field of a round free jet”, Physics of Fluids, vol, 14, N° 2.

Menter F.R., 1994, “Two-Equation Eddy Viscosity Turbulence Models for Engineering Applications”, AIAA Journal, 32(8):1598-1605.

Merci B., Dick E., 2002, “Predictive capabilities of an improved cubic k-e model for inert steady flows”, Flow, Turbulence and Combustion, vol. 68, pp 335-358.

Olsson M., Fuchs L., 1996, “Large eddy Simulation of the proximal region of a spatially developing circular jet”, Physics of Fluids, vol. 8, N° 8.

Panchapakesan N.R., Lumley J.L., 1993, “Turbulence Measurements in axisymmetric jets of air and helium. Part 1. Air jet”. J. Fluid Mechanics, vol. 246, 197.

Patankar, 1980, “Numerical Heat Transfer and Fluid Flow”, Hemisphere Publishing Corporation.

Shih T. –H., Liou W.W., Shabbir A., Yang Z., Zhu J., 1995, “A New *k*-ε Eddy Viscosity Model for High Reynolds Number Turbulent Flows – Model Development and Validation”, Computers Fluids, 24(3): 227-238.

Speziale, C. G., Abid, R., and Anderson, E. C., 1992, “Critical evalution of two-equation models for near-wall turbulence”, AIAA J., 30, pp. 324-331.

Weisgraber, T.H., Liepmann, D., 1998, “Turbulent structure during transition to self-similarity in a round jet”, Experiments in Fluids, vol. 24, pp 210-224.

Wygnanski, I., Fiedler H. E., 1969, “Some measurements in the self preserving jet”, Journal Fluid Mechanics, vol.38, 577-612.

9. Responsibility notice

The authors are the only responsible for the printed material included in this paper.